Angewandte Chemie
Eine Zeitschrift der Gesellschaft Deutscher Chemiker

Supporting Information

# Scalable Synthesis of Robust MOF for Challenging Ethylene Purification and Propylene Recovery with Record Productivity

*G.-D. Wang, Y.-Z. Li, R. Krishna, W.-Y. Zhang, L. Hou*, Y.-Y. Wang, Z. Zhu*

Supporting Information

69451 Weinheim, Germany

# Scalable Synthesis of Robust MOF for Challenging Ethylene Purification and Propylene Recovery with Record Productivity

Gang-Ding Wang,[+,a] Yong-Zhi Li,[+,a,c] Rajamani Krishna,[b] Wen-Yan Zhang,[a] Lei Hou,*[a] Yao-Yu Wang,[a] and Zhonghua Zhu[d]

**Abstract:** Ethylene ($C_2H_4$) purification and propylene ($C_3H_6$) recovery are highly relevant in polymer synthesis, yet developing physisorbents for these industrial separation faces the challenges of merging easy scalability, economic feasibility, high moisture stability with great separation efficiency. Herein, we reported a robust and scalable MOF (MAC-4) for simultaneous recovery of $C_3H_6$ and $C_2H_4$. Through creating nonpolar pores decorated by accessible N/O sites, MAC-4 displays top-tier uptakes and selectivities for $C_2H_6$ and $C_3H_6$ over $C_2H_4$ at ambient conditions. Molecular modelling combined with infrared spectroscopy revealed that $C_2H_6$ and $C_3H_6$ molecules were trapped in the framework with stronger contacts relative to $C_2H_4$. Breakthrough experiments demonstrated exceptional separation performance for binary $C_2H_6/C_2H_4$ and $C_3H_6/C_2H_4$ as well as ternary $C_3H_6/C_2H_6/C_2H_4$ mixtures, simultaneously affording record productivities of 27.4 and 36.2 L $kg^{-1}$ for high-purity $C_2H_4$ (≥ 99.9 %) and $C_3H_6$ (≥ 99.5 %). MAC-4 was facilely prepared at deckgram-scale under reflux condition within 3 hours, making it as a smart MOF to address challenging gas separations.

**DOI: 10.1002/anie.2023XXXXX**

# Table of Contents

## Materials and general methods

The reagents were purchased commercially. Thermalgravimetric analyses (TGA) were tested in a nitrogen stream using a Netzsch TG209F3 equipment (10 °C $min^{-1}$). Powder X-ray diffraction (PXRD) data were recorded on a Bruker D8 ADVANCE X-ray powder diffractometer (Cu Kα, λ = 1.5418 Å). Water sorption was collected by Quantachrome Vstar vapor adsorption equipment. Sorption measurements were performed with an automatic volumetric sorption apparatus (Micrometrics TriStar II 3020), in which the sample was activated at 393 K under vacuum for 4 hours. Breakthrough experiments were performed on a Quantachrome dynaSorb BT equipment. All the IR spectroscopic data are recorded in INVENIO S ATR-FTIR spectrometer.

## Synthesis of MAC-4

### Solvothermal synthesis of MAC-4 crystals

MAC-4 crystal was synthesized according to a previously published report.[1] The solution of 0.3 mmol 3,5-dimethyl-1,2,4-triazolate (Hdmtrz) (0.028 g) and 0.3 mmol isophthalic acid ($H_2$ipa) (0.049 g) in 5 mL of N, N-dimethylformamide (DMF) was added to the solution 5 mL DMF containing 0.45 mmol $Zn(OAc)_2{\cdot}2H_2O$ (0.089 g). The next solvothermal reactions heated at 140 °C for 3 days yielded MAC-4 crystals.

### Scale-up synthesis of MAC-4 microcrystalline

The deckgram-scale synthesis of MAC-4 was performed under reflux conditions. 54 mmol $Zn(OAc)_2{\cdot}2H_2O$ (10.68 g), 36 mmol Hdmtrz (3.36 g), 36 mmol $H_2$ipa (5.88 g) were stirred in DMF (300 mL) until it was fully dissolved (Figure 1a). Then the solutions were refluxed at 120 °C for 3 hours. The white microcrystalline of MAC-4 was collected through filtration, and then dried in air environment (Yield: 10.2 g, 77.7% based on $Zn^{2+}$ ions) (Figure 1b). Note, the DMF can be recovered by filtrating for continued synthesis of MAC-4 at least three cycles.

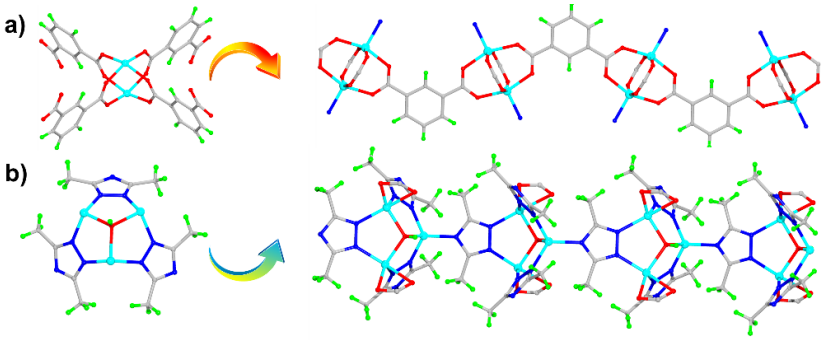


**Figure S1.** a) 1D chains composed of $[Zn_2(COO)_4]$ SBUs; b) 1D chains composed of $[Zn_3(OH)(dmtrz)_3]$ SBUs.

## Powder X-ray diffraction (PXRD)

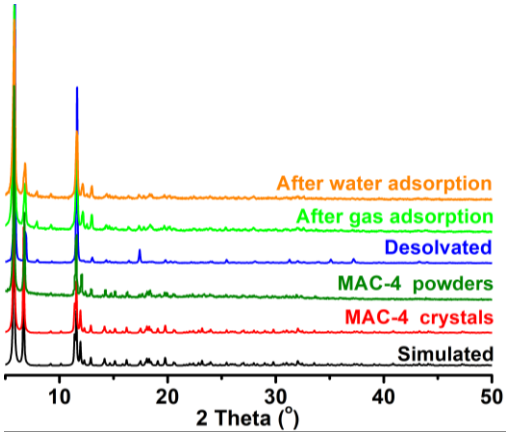


**Figure S2.** PXRD patterns of MAC-4.

## Thermogravimetric analysis (TGA)

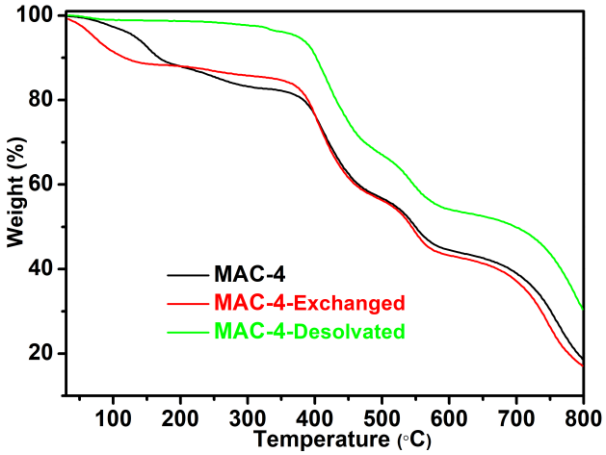


**Figure S3.** TGA curves of as-synthesized, exchanged, and desolvated samples of MAC-4.

## $N_2$ adsorption isotherms

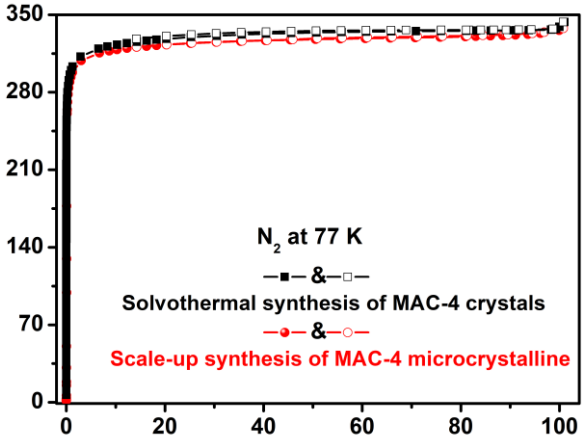


**Figure S4.** Comparison of $N_2$ adsorption isotherms (77 K) of MAC-4 synthesized by different methods.

## Water adsorption isotherms

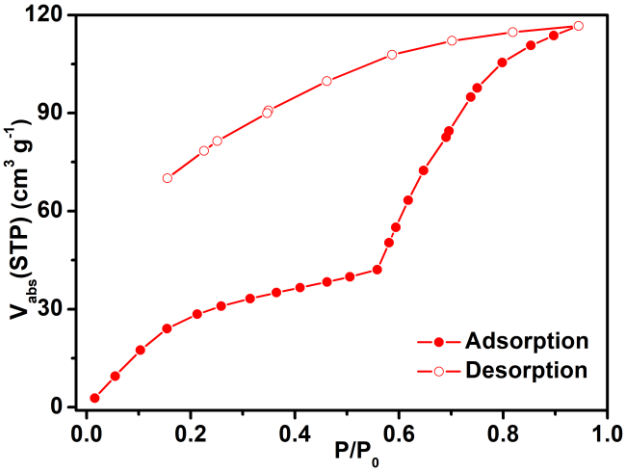


**Figure S5.** Water vapor adsorption and desorption isotherm of MAC-4 at 298 K.

## Gas adsorption isotherms

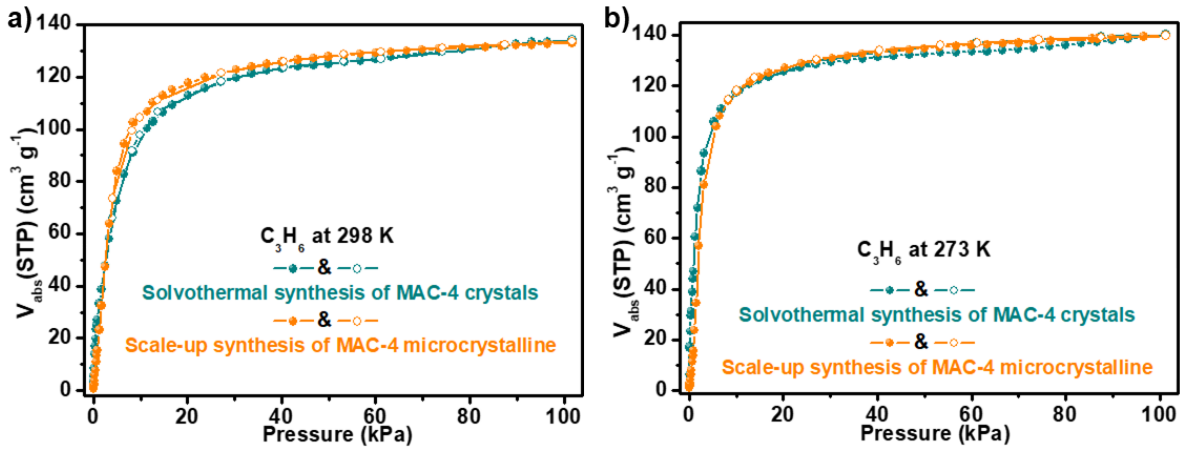


**Figure S6.** The comparison of adsorption isotherm curves of solvothermal synthesis of MAC-4 crystals samples and scale-up synthesis of MAC-4 microcrystalline samples for $C_3H_6$ at 298 K a); and 273 K b).

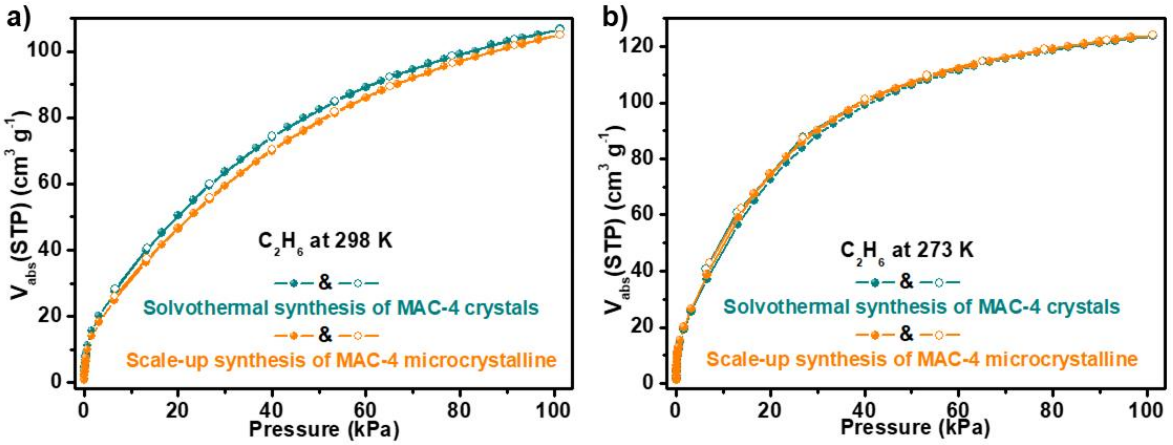


**Figure S7.** The comparison of adsorption isotherm curves of solvothermal synthesis of MAC-4 crystals samples and scale-up synthesis of MAC-4 microcrystalline samples for $C_2H_6$ at 298 K a); and 273 K b).

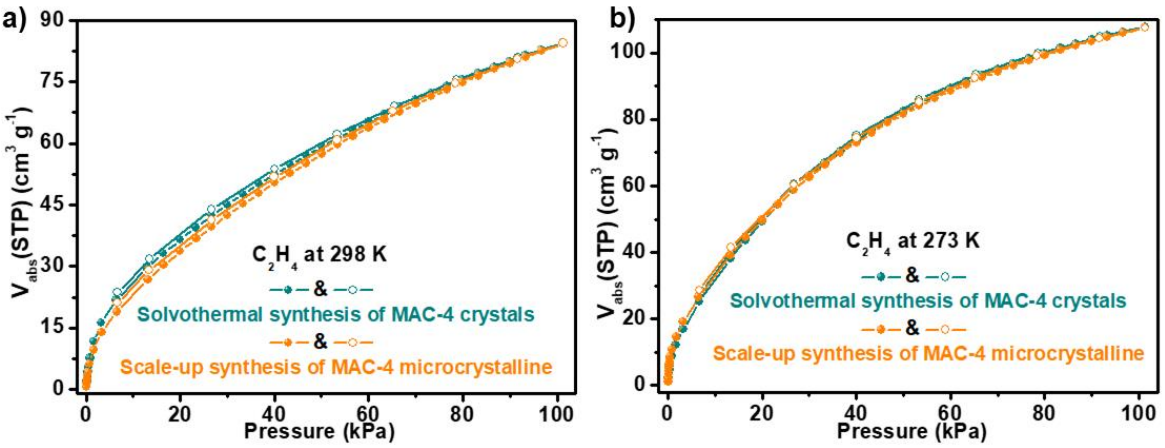


**Figure S8.** The comparison of adsorption isotherm curves of solvothermal synthesis of MAC-4 crystals samples and scale-up synthesis of MAC-4 microcrystalline samples for $C_2H_4$ at 298 K a); and 273 K b).

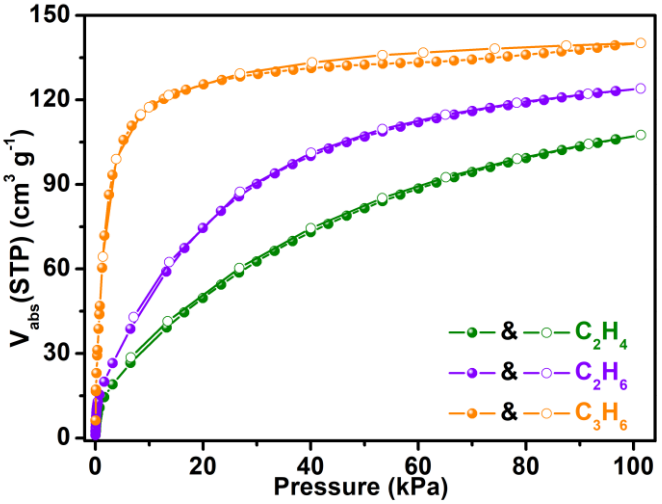


**Figure S9.** $C_3H_6$, $C_2H_4$ and $C_2H_6$ adsorption isotherms of MAC-4 at 273 K.

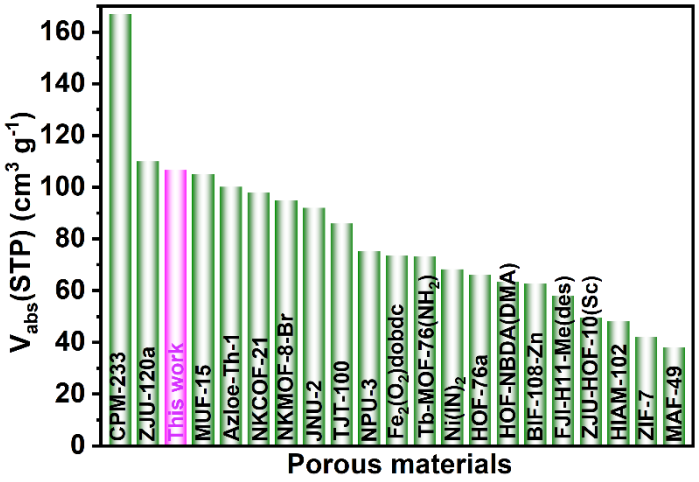


**Figure S10.** Comparisons of $C_2H_6$ uptakes in MAC-4 and leading materials at 298 K.

## Fitting adsorption heat of pure component isotherms

The unary isotherms for $C_3H_6$, $C_2H_6$, and $C_2H_4$, measured at two different temperatures 273 K, and 298 K in MAC-4 were fitted with excellent accuracy using the dual-site Langmuir model, where we distinguish two distinct adsorption sites A and B:

$$q=\frac{q_{sat,A}b_Ap}{1+b_Ap}+\frac{q_{sat,B}b_Bp}{1+b_Bp} \quad \text{(S1)}$$

In eq ), the Langmuir parameters $b_A$, $b_B$ are both temperature dependent

$$b_A=b_{A0}\,exp\left(\frac{E_A}{RT}\right);\quad b_b=b_{B0}\,exp\left(\frac{E_B}{RT}\right) \quad \text{(S2)}$$

In eq (S2), $E_A$, $E_B$ are the energy parameters associated with sites A, and B, respectively.

The unary isotherm fit parameters are provided in **Fehler! Verweisquelle konnte nicht gefunden werden.**.

The isosteric heat of adsorption, $Q_{st}$, is defined as

$$Q_{st}=-RT^2\left(\frac{\partial \ln p}{\partial T}\right)_q \quad \text{(S3)}$$

where, the derivative in the right member of eq (S3) is determined at constant adsorbate loading, $q$. the derivative was determined by analytic differentiation of the combination of eq ), eq (S2), and eq (S3).

**Table S1**. Dual-site Langmuir fits for $C_3H_6$, $C_2H_6$, and $C_2H_4$ in MAC-4.

| | Site A | | | Site B | | |
|---|---|---|---|---|---|---|
| | $q_{A,sat}$ mol/kg | $b_{A0}$ $Pa^{-1}$ | $E_A$ kJ $mol^{-1}$ | $q_{B,sat}$ mol/kg | $b_{B0}$ $Pa^{-1}$ | $E_B$ kJ $mol^{-1}$ |
| $C_3H_6$ | 5.4 | 4.253E-10 | 31.7 | 0.7 | 4.062E-07 | 24 |
| $C_2H_6$ | 6.3 | 8.897E-09 | 19 | 0.6 | 2.389E-07 | 23 |
| $C_2H_4$ | 6.8 | 5.481E-09 | 18 | 0.7 | 1.012E-06 | 17 |

## Gas adsorption cycles

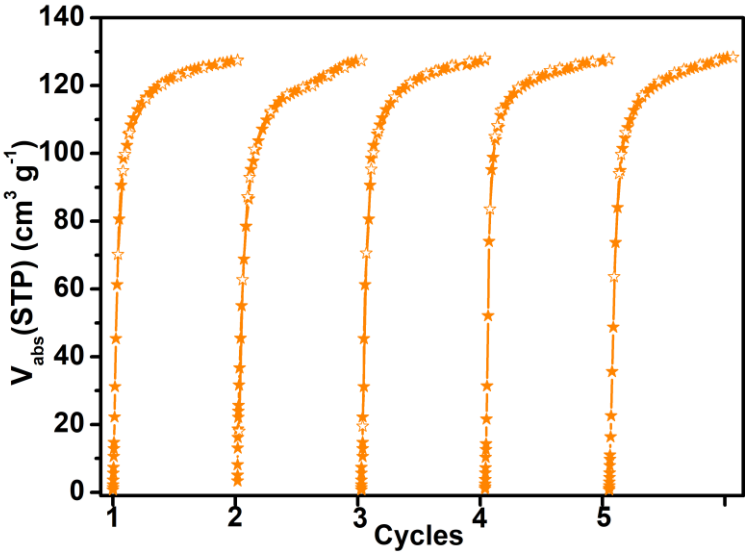


**Figure S11**. Repetitive $C_3H_6$ adsorption curves at 298 K.

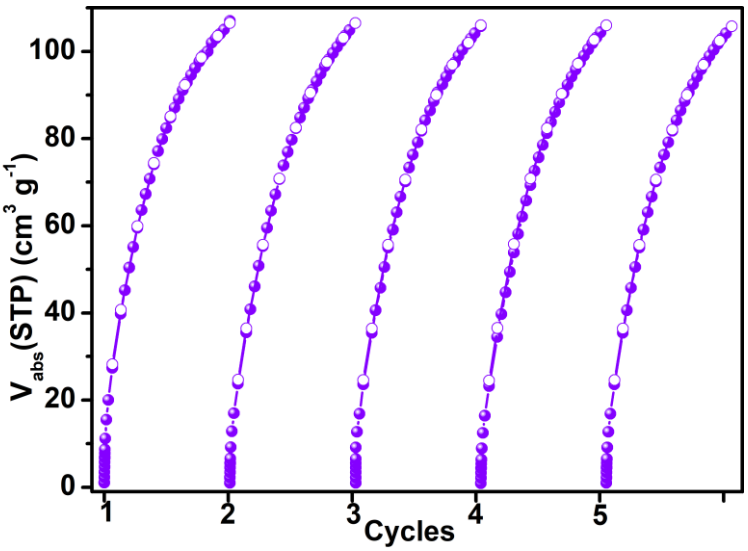


**Figure S12**. Repetitive $C_2H_6$ adsorption curves at 298 K.

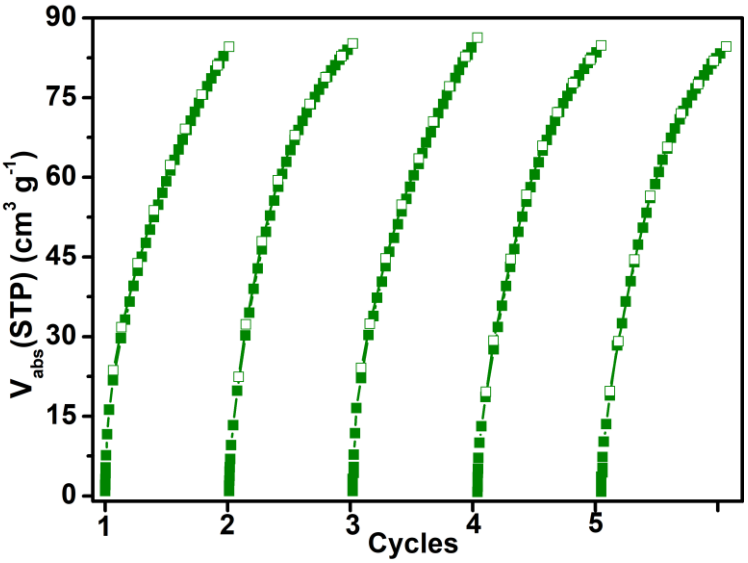


**Figure S13**. Repetitive $C_2H_4$ adsorption curves at 298 K.

## Estimation of production cost of MAC-4

**Table S2.** The raw material cost of various adsorbents.

| Material | Price ($ $g^{-1}$) | Source |
|---|---|---|
| $Zn(OAc)_2 \cdot 2H_2O$ | 0.003 $ $g^{-1}$ | Greagent |
| Hdmtrz | 2.469 $ $g^{-1}$ | Adamas |
| $H_2IPA$ | 0.007 $ $g^{-1}$ | Adamas |
| DMF | 0.018 $ $mL^{-1}$ | Sigma-Aldrich |
| MAC-4 | 1.349 $ $g^{-1}$ | Synthesis |

Note: Material cost was calculated by using the required amounts of metal salts and organic ligands precursor. Additionally, the cost of the operation and utility cost for hydrothermal reaction, filtrate, and drying, etc. are not considered.

## Gas selectivity prediction via IAST

The experimental isotherm data for pure $C_3H_6$, $C_2H_4$ and $C_2H_6$ were fitted using a dual-site Langmuir-Freundlich (L-F) model:

$$q = \frac{a_1 * b_1 * P^{c_1}}{1 + b_1 * P^{c_1}} + \frac{a_2 * b_2 * P^{c_2}}{1 + b_2 * P^{c_2}}$$

Where *q* and *p* are adsorbed amounts and the pressure of component i, respectively.

The adsorption selectivities for binary mixtures defined by

$$S_{i/j} = \frac{x_i * y_j}{x_j * y_i}$$

wererespectively calculated using the Ideal Adsorption Solution Theory (IAST). Where $x_i$ is the mole fraction of component *i* in the adsorbed phase and $y_i$ is the mole fraction of component i in the bulk.

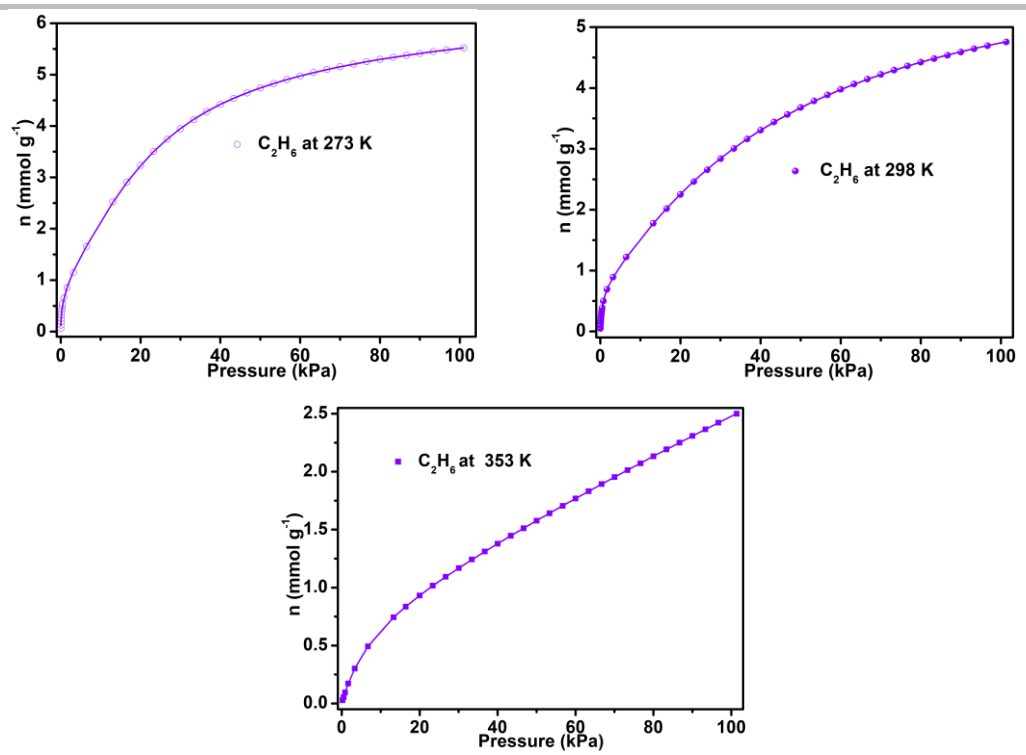


**Figure S14**. $C_2H_6$ adsorption isotherms of MAC-4 with fitted by dual L-F model, 273 K: a1 = 2.44243, b1 = 0.00296, c1 = 1.89301, a2 = 5.86278, b2 = 0.13443, c2 = 0.47539, Chi^2 = 0.00041, R^2 = 0.99992; 298 K: a1 = 5.58896, b1 = 0.01072, c1 = 1.18007, a2 = 0.77584, b2 = 1.89883, c2 = 0.97692, Chi^2 = 0.00002, R^2 = 0.99999; 353 K: a1 = 11.54749, b1 = 0.00088, c1 = 1.14146, a2 = 0.87088, b2 = 0.12614, c2 = 1.00959, Chi^2 = 6.818E-7, R^2 = 1.

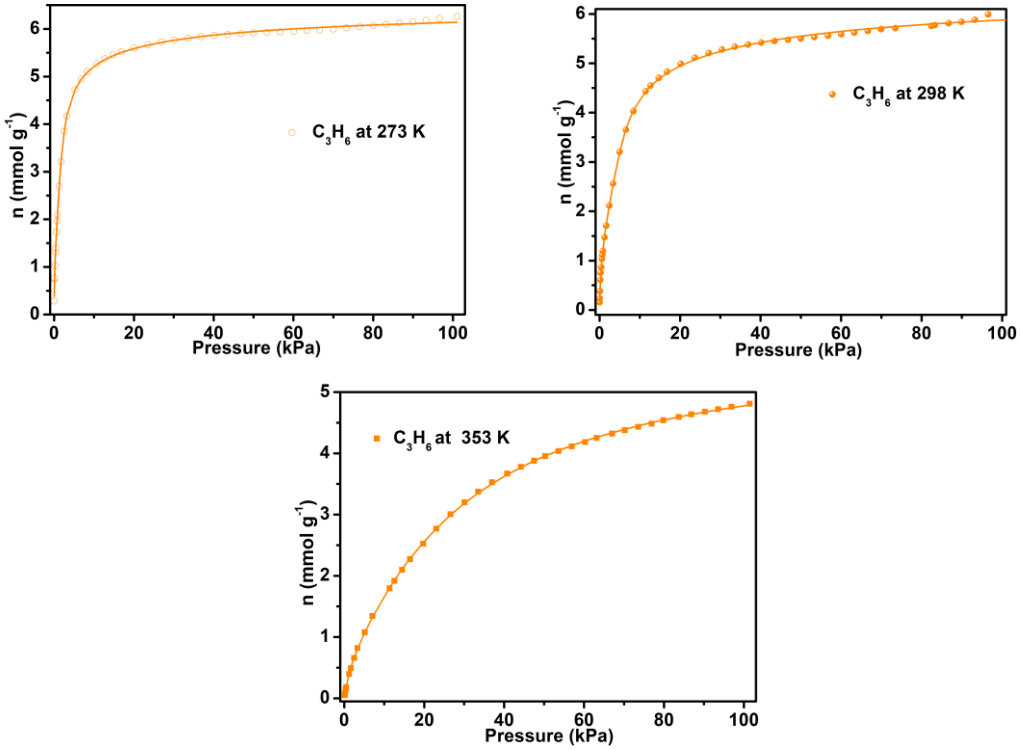


**Figure S15**. $C_3H_6$ adsorption isotherms of MAC-4 with fitted by dual L-F model, 273 K: a1 = 4.63475, b1 = 0.66052, c1 = 0.56825, a2 = 1.96456, b2 = 0.34334, c2 = 2.14875, Chi^2 = 0.00154, R^2 = 0.99962; 298 K: a1 = 5.36762, b1 = 0.32974, c1 = 0.64812, a2 = 1.22382, b2 = 0.0082, c2 = 2.97596, Chi^2 = 0.00201, R^2 = 0.99957; 353 K: a1 = 5.06649, b1 = 0.01649, c1 = 1.20353, a2 = 0.68958, b2 = 0.60603, c2 = 1.08723, Chi^2 = 0.00018, R^2 = 0.99994.

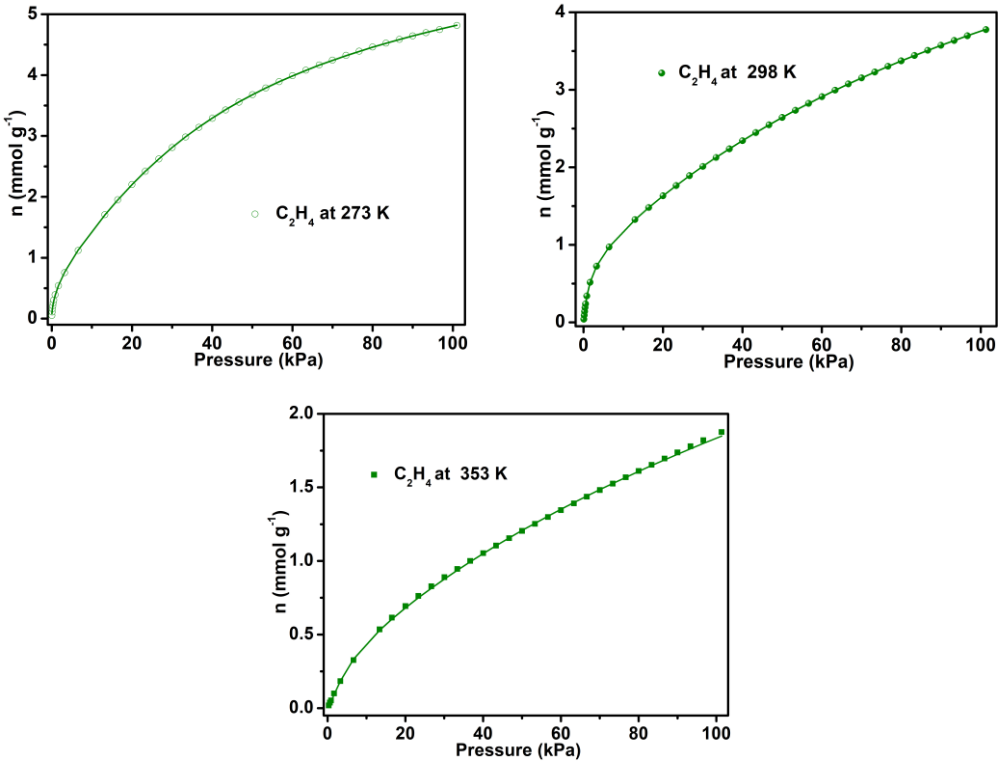


**Figure S16**. $C_2H_4$ adsorption isotherms of MAC-4 with fitted by dual L-F model, 273 K: a1 = 9.43954, b1 = 0.04569, c1 = 0.52526, a2 = 1.87921, b2 = 0.002, c2 = 1.73163, Chi^2 = 0.00008, R^2 = 0.99998; 298 K: a1 = 6.88414, b1 = 0.00606, c1 = 1.04001, a2 = 0.87108, b2 = 0.64858, c2 = 0.97491, Chi^2 = 3.3222E-6, R^2 =1; 353 K: a1 = 6.50703, b1 = 0.00649, c1 = 0.8607, a2 = 0.17791, b2 = 0.07126, c2 = 1.81603, Chi^2 = 0.00011, R^2 = 0.99973.

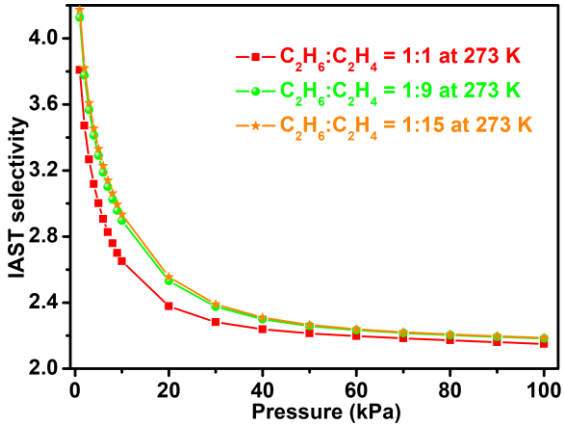


**Figure S17**. IAST selectivity curves of MAC-4 for $C_2H_6/C_2H_4$ at 273 K.

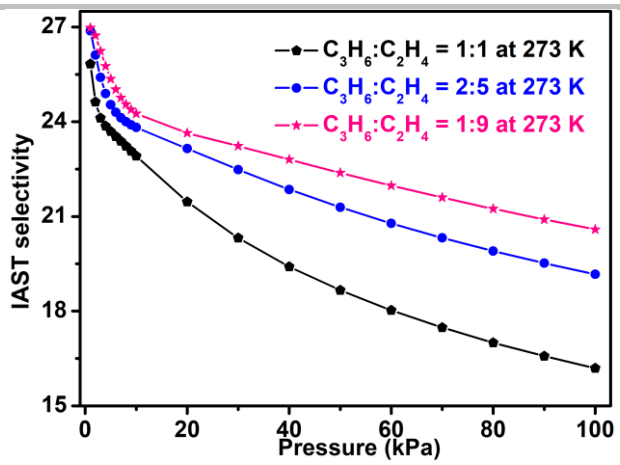


**Figure S18**. IAST selectivity curves of MAC-4 for $C_3H_6/C_2H_4$ at 273 K.

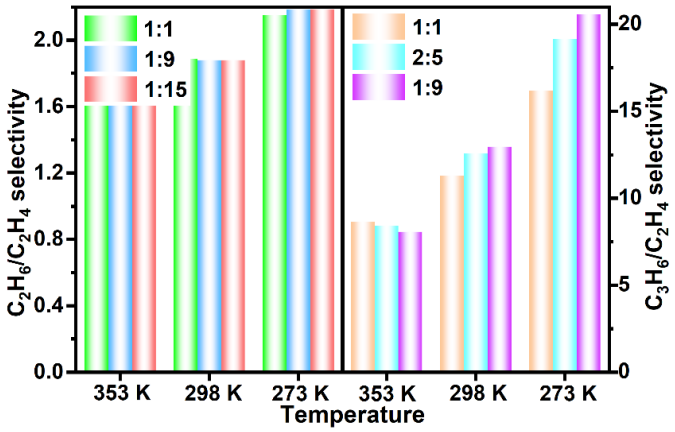


**Figure S19**. IAST selectivity values of MAC-4 for $C_2H_6/C_2H_4$ and $C_3H_6/C_2H_4$ at 353, 298, and 273 K.

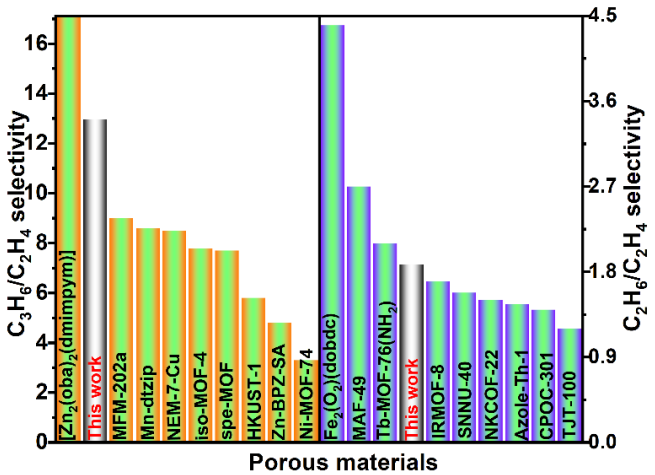


**Figure S20**. Comparison of $C_3H_6/C_2H_4$ (left) and $C_2H_6/C_2H_4$ (right) selectivities in MAC-4 and some benchmark adsorbents at 298 K.

## Separation potential

For separation of binary 50/50 $C_2H_6(1)/C_2H_4(2)$, 50/50 $C_3H_6(1)/C_2H_4(2)$ mixtures, the maximum productivity of purified $C_2H_4$ that is theoretically achievable in a fixed bed adsorber is determined by the metric defined by Krishna[2,3] as the separation potential, $\Delta Q$, derived on the basis of the shock wave model

For 50/50 $C_2H_6(1)/C_2H_4(2)$ mixtures: $\Delta Q=(q_{C2H6})\frac{50}{50}-q_{C2H4}$ ; For 50/50 $C_3H_6(1)/C_2H_4(2)$ mixtures: $\Delta Q=(q_{C3H6})\frac{50}{50}-q_{C2H4}$

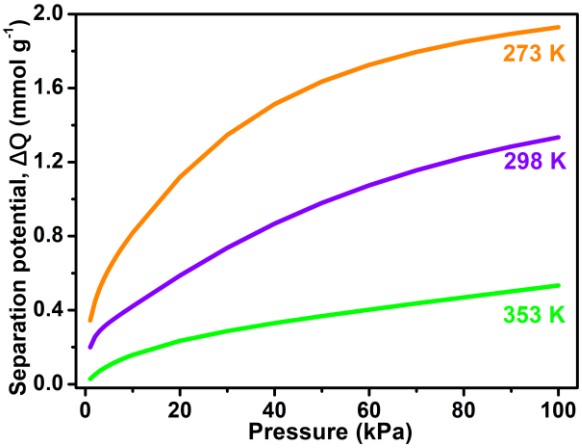


**Figure S21**. Separation potential of MAC-4 for $C_2H_6/C_2H_4$ mixtures at 273, 298, and 353K.

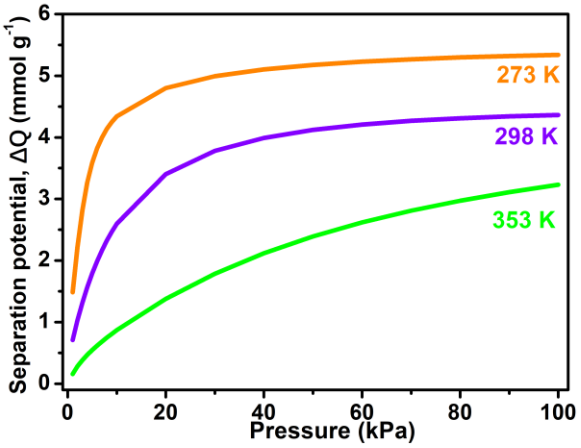


**Figure S22**. Separation potential of MAC-4 for $C_3H_6/C_2H_4$ mixtures at 273, 298, and 353K.

## GCMC simulation

Grand canonical Monte Carlo (GCMC) simulations were performed for the gas adsorption in the framework by the Sorption module of Material Studio (Accelrys. Materials Studio Getting Started). The framework was considered to be rigid, and the optimized gas molecules were used. The partial charges for atoms of the framework were derived from QEq method and QEq neutral 1.0 parameter. One unit cell was used during the simulations. The interaction energies between the gas molecules and framework were computed through the Coulomb and Lennard-Jones 6-12 (LJ) potentials. All parameters for the atoms were modeled with the universal force field (UFF) embedded in the MS modeling package. A cutoff distance of 12.5 Å was used for LJ interactions, and the Coulombic interactions were calculated by using Ewald summation. For each run, the $3 \times 10^6$ maximum loading steps, $3 \times 10^6$ production steps were employed. The binding energy was calculated by following equation: $E_{bind} = E_{framework+gas} - E_{framework} - E_{gas}$, in which $E_{framework+gas}$ is the total energy of the framework and the adsorbed gas molecule, $E_{framework}$ and $E_{gas}$ are the energies of the framework and gas molecule. The exchange-correlation functional used in calculations was in the framework of the generalized gradient approximation (GGA) proposed by Perdew, Burke and Ernzerhof (PBE). DNP basis set was used to describe the atomic orbital. The SCF convergence was set to $1\times10^{-6}$.

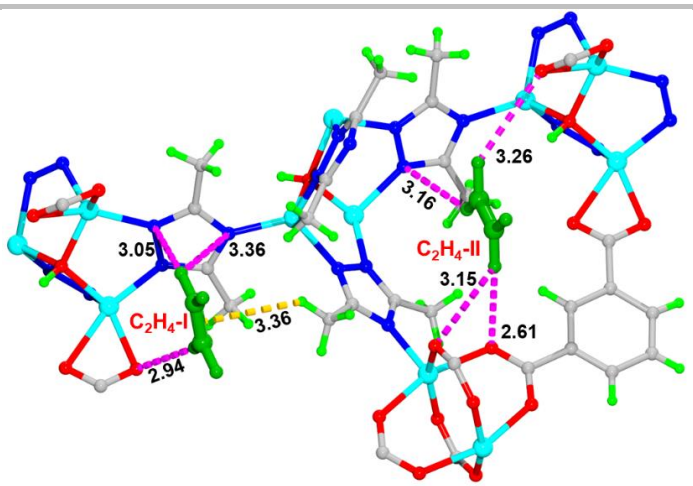


**Figure S23**. Adsorption sites for $C_2H_4$-I and $C_2H_4$-II at 298 K under 100 kPa (H, green; Zn, turquiose; C, gray; O, red; N, blue).

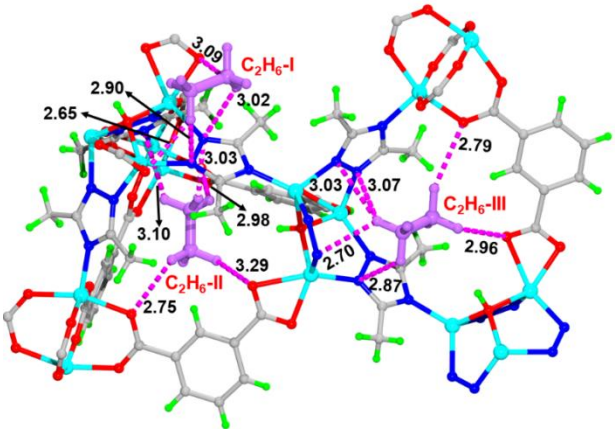


**Figure S24**. Adsorption sites for $C_2H_6$-I, $C_2H_6$-II and $C_2H_6$-III at 298 K under 100 kPa (H, green; Zn, turquiose; C, gray; O, red; N, blue).

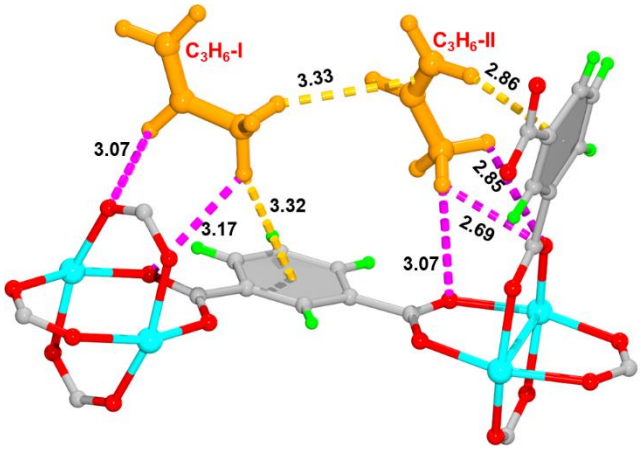


**Figure S26**. Adsorption sites for $C_3H_6$-I and $C_2H_6$-II at 298 K under 100 kPa (H, green; Zn, turquiose; C, gray; O, red; N, blue).

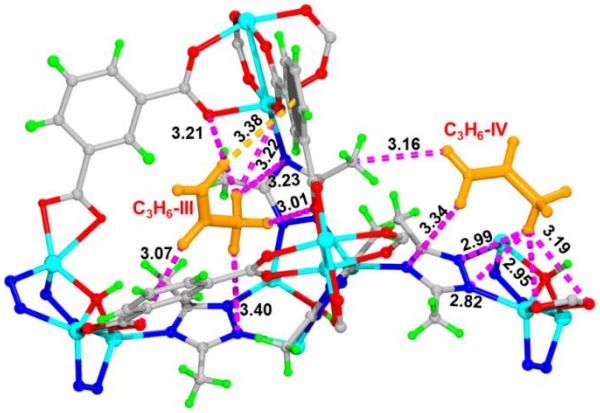


**Figure S26**. Adsorption sites for $C_3H_6$-I and $C_2H_6$-IV at 298 K under 100 kPa (H, green; Zn, turquiose; C, gray; O, red; N, blue).

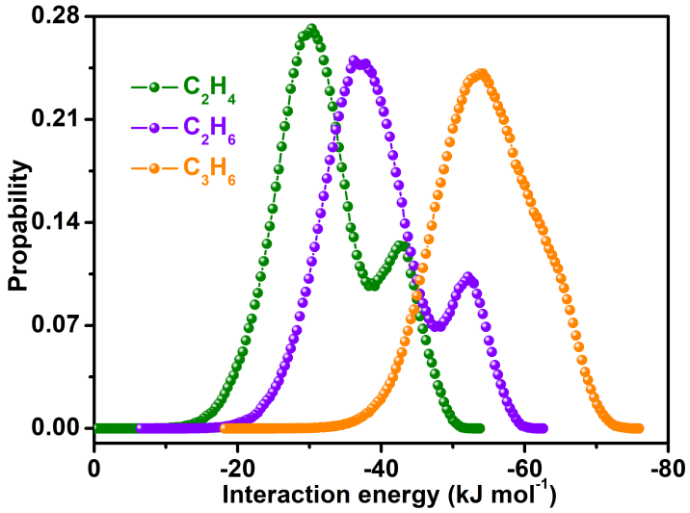


**Figure S27**. Interaction energy distribution of $C_2H_4$, $C_2H_6$, and $C_3H_6$ in the MAC-4.

## Breakthrough experiments

The breakthrough experiments were performed on the Quantachrome dynaSorb BT equipments at 273, 298 and 353 K and 100 kPa with Ar as the carrier gas. The activated MAC-4 (about 0.88 g) was filled into a packed column of ϕ 4.2 mm × 80 mm, and then the packed column was washed with Ar at a rate of 7 mL $min^{-1}$ at 343 K for 50 minutes to further activate the samples. Between two breakthrough experiments, the adsorbent was regenerated by Ar flow of 7 mL $min^{-1}$ for 35 min at 343 K to guarantee a complete removal of the adsorbed gas.

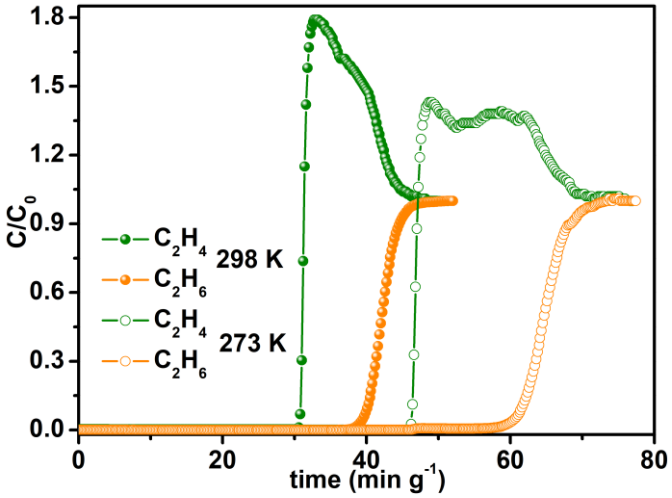


**Figure S28.** Breakthrough curves of MAC-4 for equimolar $C_2H_6/C_2H_4$ (10/10, v/v) mixtures at 298 and 273 K with Ar as the carrier gas (80%, vol%).

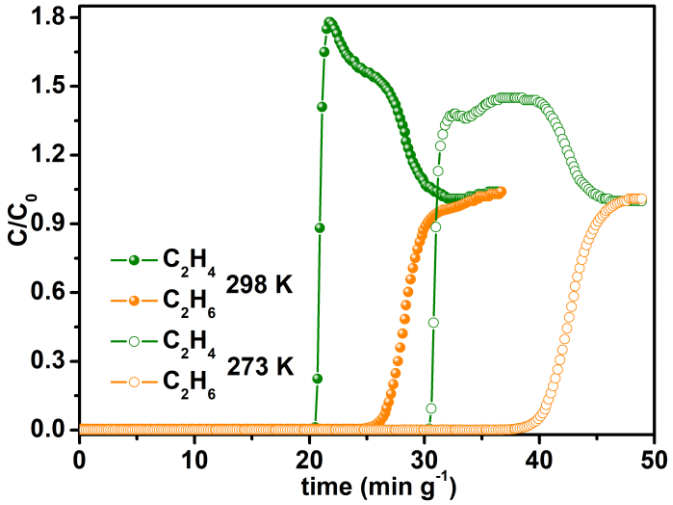


**Figure S29.** Breakthrough curves of MAC-4 for equimolar $C_2H_6/C_2H_4$ (20/20, v/v) mixtures at 298 and 273 K with Ar as the carrier gas (60%, vol%).

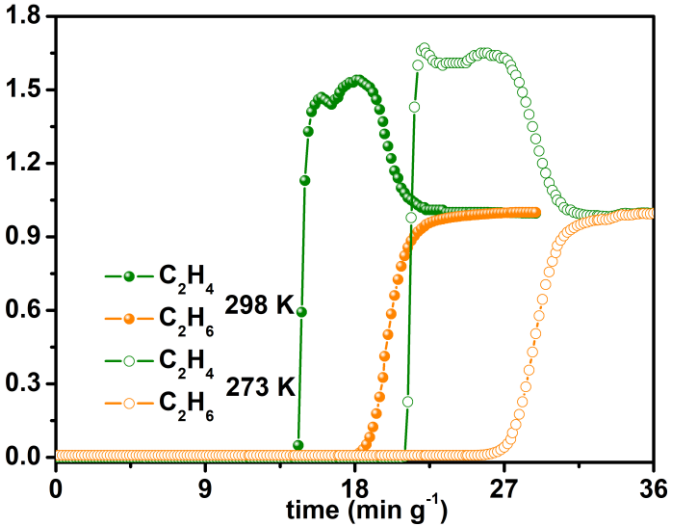


**Figure S30.** Breakthrough curves of MAC-4 for equimolar $C_2H_6/C_2H_4$ (30/30, v/v) mixtures at 298 and 273 K with Ar as the carrier gas (40%, vol%).

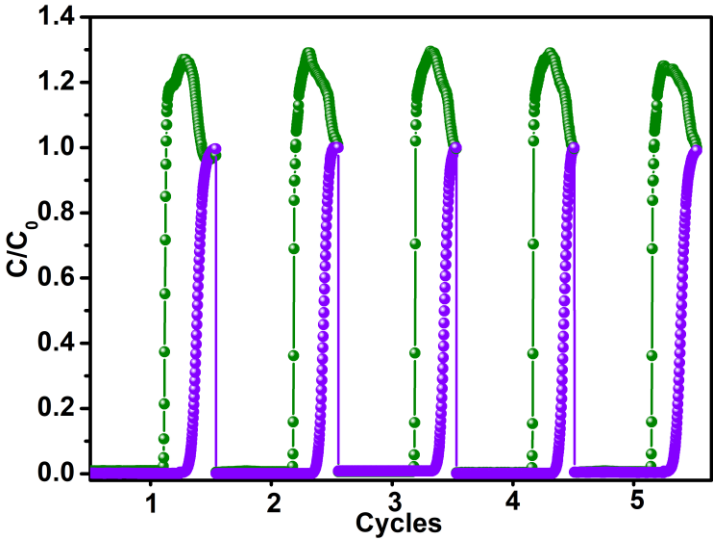


**Figure S31.** Breakthrough cycles of MAC-4 for $C_2H_6/C_2H_4$ mixtures at 298 K.

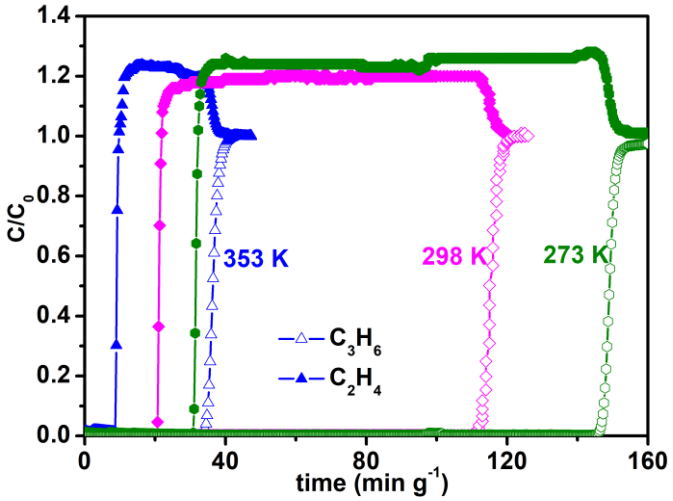


**Figure S32.** Breakthrough curves for $C_3H_6/C_2H_4$ (v/v, 10/25) mixtures at 353, 298 and 273 K.

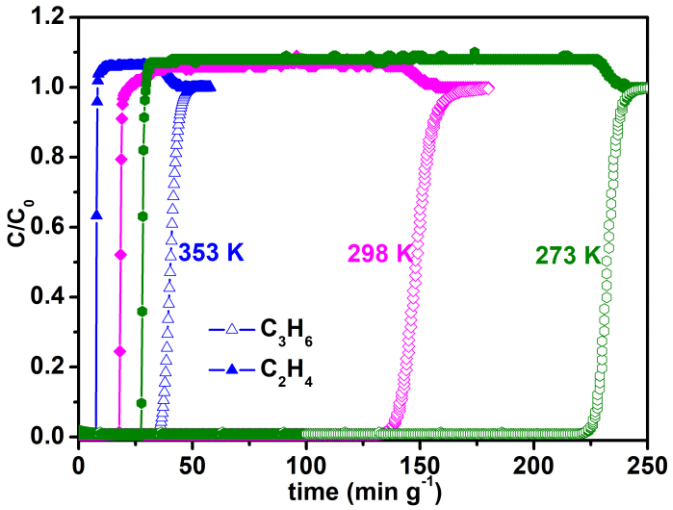


**Figure S33.** Breakthrough curves for $C_3H_6/C_2H_4$ (v/v, 4/36) mixtures at 353, 298 and 273 K.

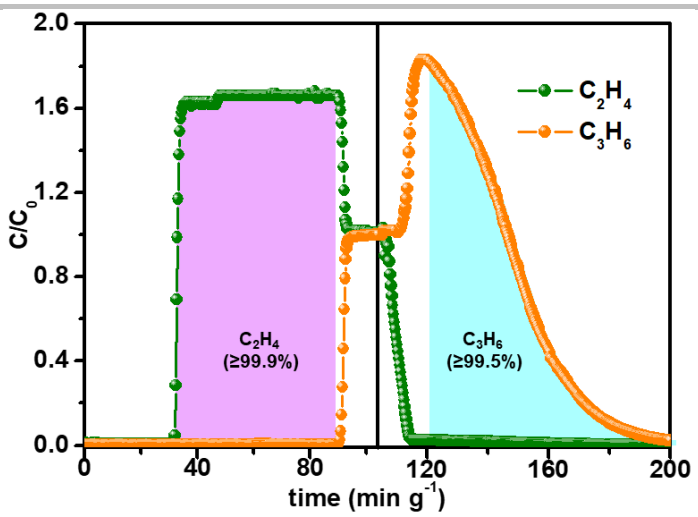


**Figure S34.** Breakthrough curves for $C_3H_6/C_2H_4$ (v/v, 20/20) mixtures at 273 K, followed by desorption curves under Ar (7 mL $min^{-1}$) sweeping at 323 K.

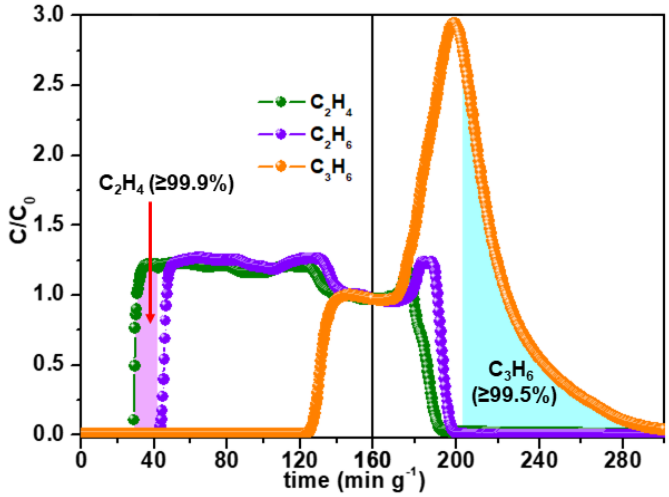


**Figure S35.** Breakthrough curves for $C_2H_6/C_3H_6/C_2H_4$ mixture (v/v/v,5/5/5) mixtures at 298 K, followed by desorption curves under Ar (7 mL $min^{-1}$) sweeping at 323 K.

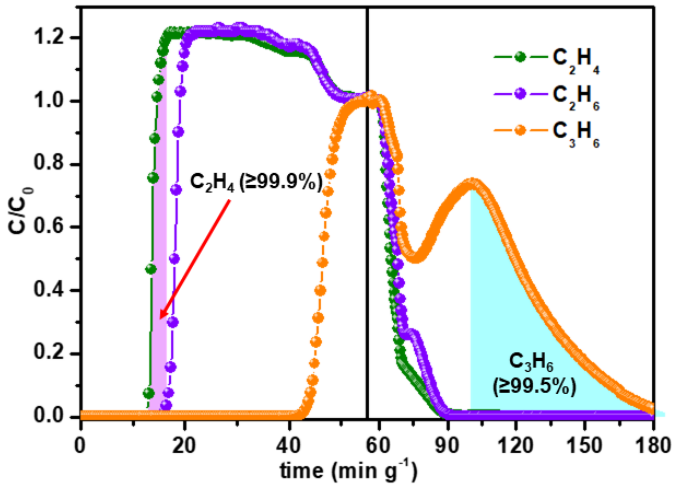


**Figure S36.** Breakthrough curves for $C_2H_6/C_3H_6/C_2H_4$ mixture (v/v/v,5/5/5) mixtures at 353 K, followed by desorption curves under Ar (7 mL $min^{-1}$) sweeping at 323 K.

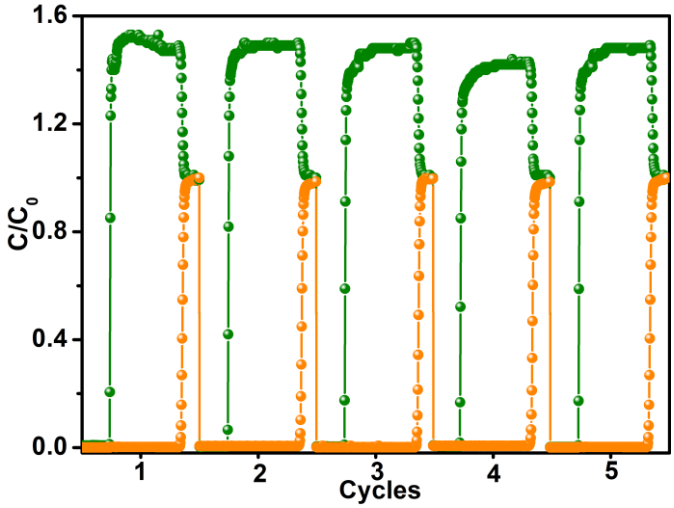


**Figure S37.** Breakthrough cycles of MAC-4 for $C_3H_6/C_2H_4$ mixtures at 298 K.

## Transient breakthrough simulations vs experiments with inert gas

The transient breakthrough experiments were conducted with mass of MAC-4 $m_{ads}$ = 0.88 g; length of packed bed, $L$ = 80 mm; diameter of packed bed= 4.2 mm. The mixtures examined were:

$C_3H_6/C_2H_4$/Ar mixtures (20/20/60 v/v) with Ar as the carrier gas, and a total flow rate of 8.0 mL $min^{-1}$ (353 K and 298 K, 100 kPa);

$C_2H_6/C_2H_4$/Ar mixtures (5/5/90, 1/9/90, and 1/15/84, v/v/v) with Ar as the carrier gas, and a total flow rate of 7 mL $min^{-1}$ (353 K and 298 K, 100 kPa);

$C_3H_6/C_2H_6/C_2H_4$/Ar mixtures (5/5/5/85, 10/2/25/63, v/v/v/v, ) with Ar as the carrier gas, and a total flow rate of 8 mL $min^{-1}$ (353 K and 298 K, 100 kPa).

Transient breakthrough simulations were carried out for the exact same set of operating conditions as in the above mentioned experiments, using the methodology described in earlier publications.[2-7] In these simulations, intra-crystalline diffusion influences are ignored. There is good match between the experiments and simulations in every case.

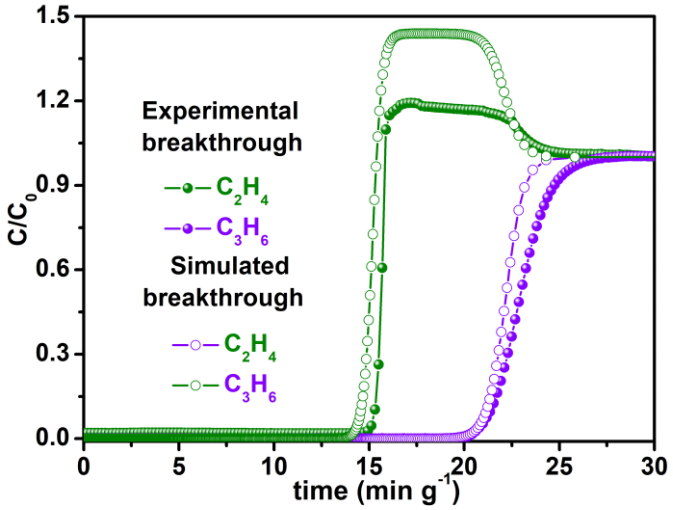


**Figure S38.** Comparison of the transient breakthrough curves and experimental breakthrough curves for $C_2H_6/C_2H_4$ (5/5) mixtures at 353 K.

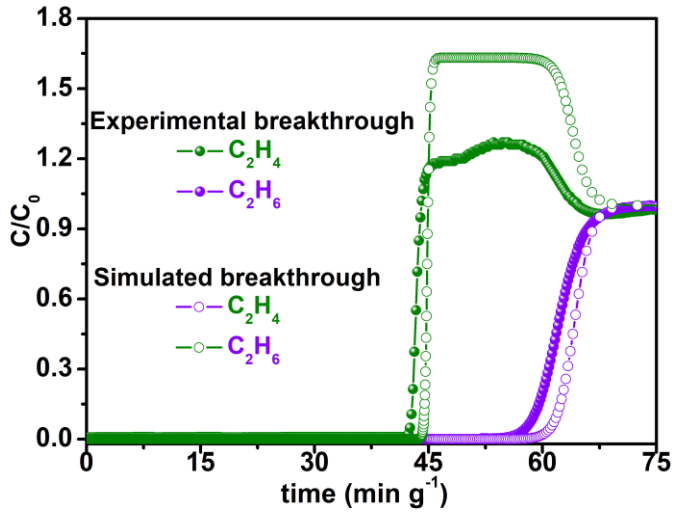


**Figure S39.** Comparison of the transient breakthrough curves and experimental breakthrough curves for $C_2H_6/C_2H_4$ (5/5) mixtures at 298 K.

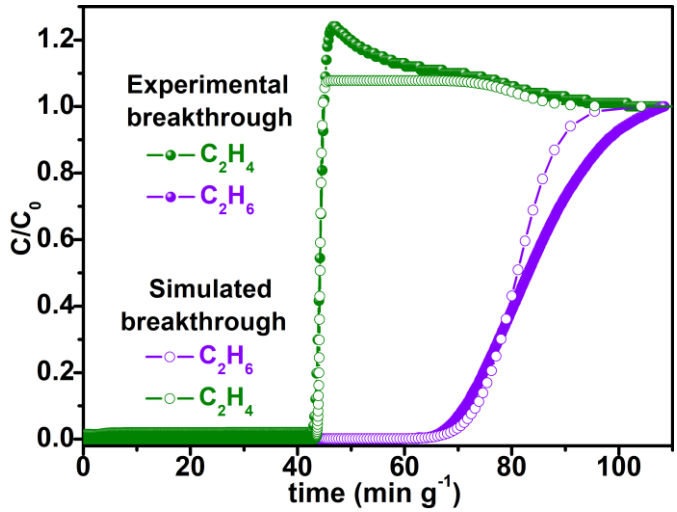


**Figure S40.** Comparison of the transient breakthrough curves and experimental breakthrough curves for $C_2H_6/C_2H_4$ (1/9) mixtures at 298 K.

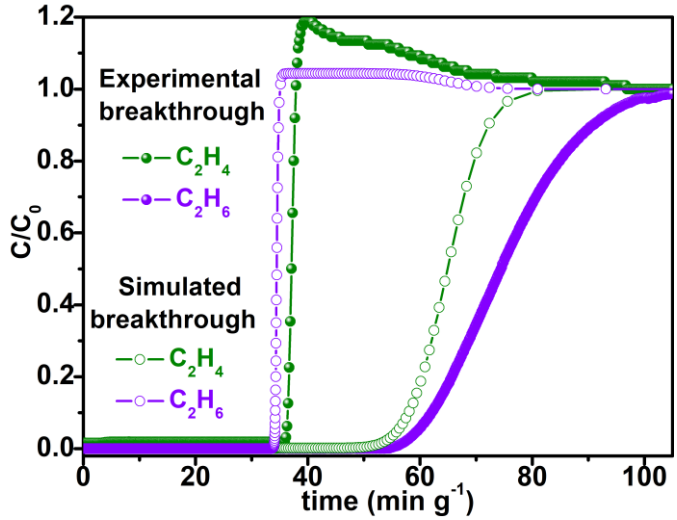


**Figure S41.** Comparison of the transient breakthrough curves and experimental breakthrough curves for $C_2H_6/C_2H_4$ (1/15) mixtures at 298 K.

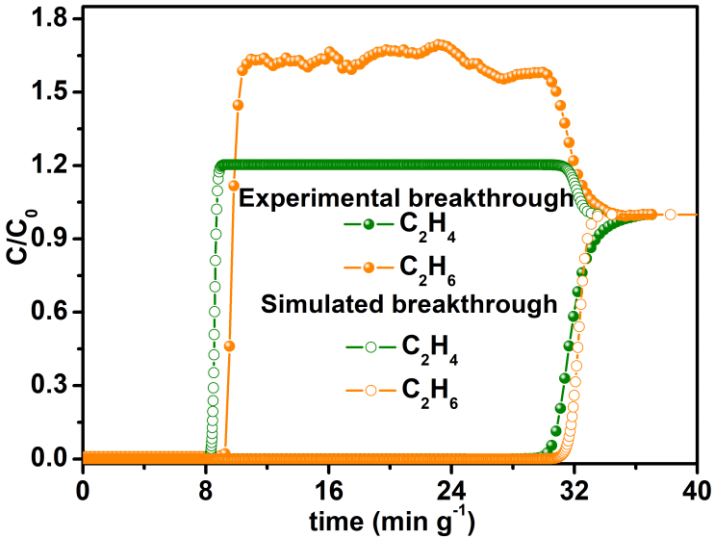


**Figure S42.** Comparison of the transient breakthrough curves and experimental breakthrough curves for $C_3H_6/C_2H_4$ (20/20) mixtures at 353 K.

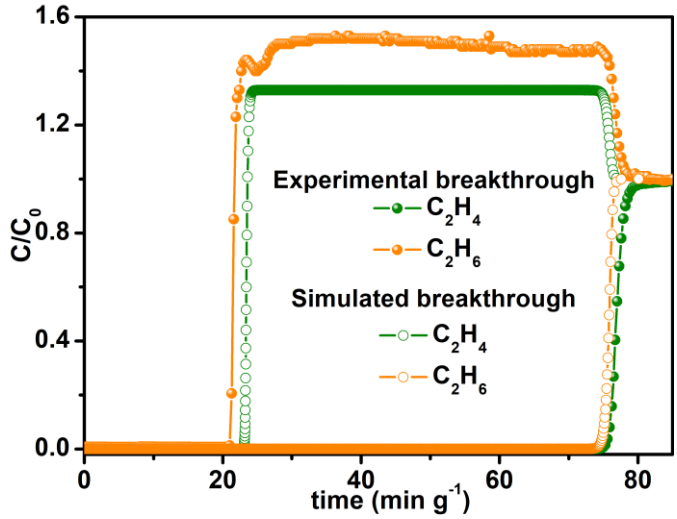


**Figure S43.** Comparison of the transient breakthrough curves and experimental breakthrough curves for $C_3H_6/C_2H_4$ (20/20) mixtures at 298 K.

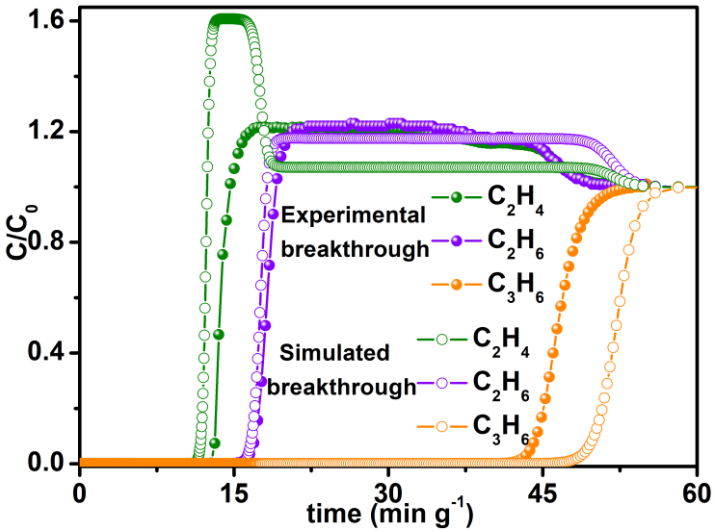


**Figure S44.** Comparison of the transient breakthrough curves and experimental breakthrough curves for $C_3H_6/C_2H_6/C_2H_4$ (5/5/5) mixtures at 353 K.

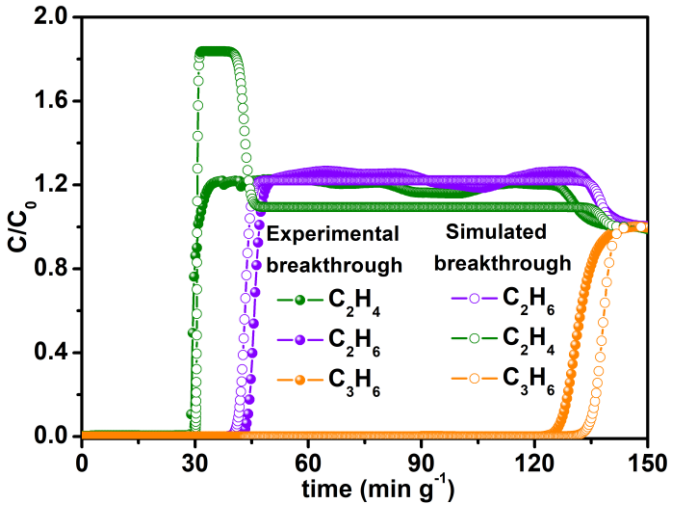


**Figure S45.** Comparison of the transient breakthrough curves and experimental breakthrough curves for $C_3H_6/C_2H_6/C_2H_4$ (5/5/5) mixtures at 298 K.

## Transient breakthrough simulations without inert gas

Having established the accuracy of the transient breakthrough simulations, a set of simulations were carried out without inert gas in a fixed bed packed with MAC-4 $m_{ads}$ = 0.88 g; length of packed bed, $L$ = 80 mm; diameter of packed bed= 4.2 mm. The total pressure is 100 kPa, and two different temperatures were used: 298 K and 353 K. The following mixtures were simulated.

50/50 $C_2H_6$(1)/$C_2H_4$(2) mixtures

50/50 $C_3H_6$(1)/$C_2H_4$(2) mixtures

33.33/33.33/33.33 $C_3H_6$(1)/$C_2H_6$(2)/$C_2H_4$(3) mixtures

The breakthrough data are presented in terms of the dimensionless concentrations at the exit of the fixed bed, $\frac{c_A}{c_{A0}}$, as function of the modified time parameter $\frac{\left(Q_0 = \text{flow rate mL min}^{-1}\right) \times (\text{time in min})}{(\text{g MOF packed in tube})} = \frac{Q_0 t}{m_{ads}} = mL\ g^{-1}$.

From the transient breakthrough simulations, the productivity of 99.9% $C_2H_4$ was determined from a material balance.

Notation:

| | |
|---|---|
| $b$ | Langmuir constant, $Pa^{-1}$ |
| $E$ | energy parameter, J $mol^{-1}$ |
| $L$ | length of packed bed adsorber, m |
| $m_{ads}$ | mass of adsorbent packed in fixed bed, g |
| $p_i$ | partial pressure of species $i$ in mixture, Pa |
| $p_t$ | total system pressure, Pa |
| $q_i$ | component molar loading of species $i$, mol $kg^{-1}$ |
| $q_t$ | total molar loading in mixture, mol $kg^{-1}$ |
| $q$ | component molar loading of species $i$, mol $kg^{-1}$ |
| $q_{sat}$ | saturation loading, mol $kg^{-1}$ |
| $Q_0$ | volumetric flow rate of gas mixture entering fixed bed, $m^3\ s^{-1}$ |
| $Q_{st}$ | isosteric heat of adsorption, kJ $mol^{-1}$ |
| $T$ | absolute temperature, K |
| $u$ | superficial gas velocity in packed bed, m $s^{-1}$ |
| $\varepsilon$ | voidage of packed bed, dimensionless |
| $\rho$ | framework density, kg $m^{-3}$ |

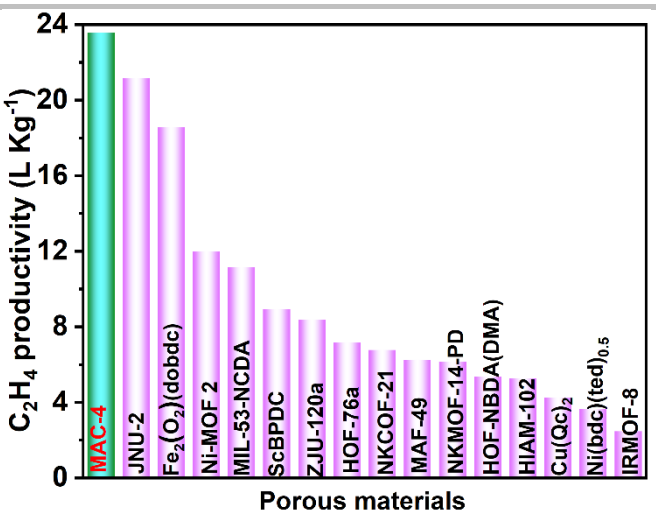


**Figure S46.** Comparison of $C_2H_4$ productivity form equimolar $C_2H_6/C_2H_4$ mixture in MAC-4 and reported porous adsorbents.

## Infrared spectroscopy study

Infrared (IR) measurements were performed on a Bruker INVENIO S ATR-FTIR spectrometer. The samples of gas-loaded MAC-4 were prepared by the method described below: The sample of MAC-4 was filled into a glass tube and heated at 140 °C under vacuum for 4h. After the sample cooling down, $C_2H_4$, $C_3H_6$, and $C_2H_6$ was introduced into the sample respectively with Micrometrics TriStar II 3020 instrument until the pressure reach to 100 kPa at 298 K and the state is maintained for two hours. Then gas loading sample were picked out for infrared measurement immediately.

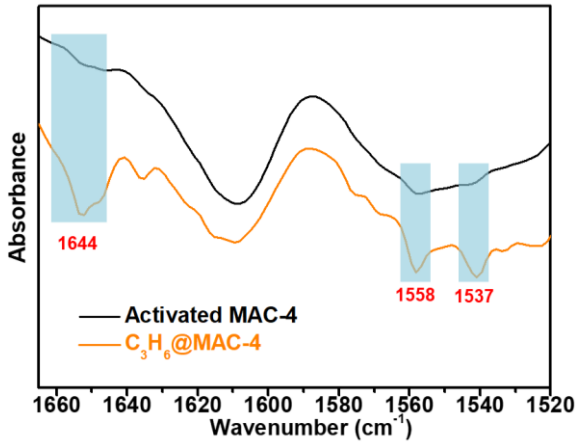


**Figure S47.** Comparison of IR spectra at 1660-1520 $cm^{-1}$ of activated and $C_3H_6$-loaded MAC-4.

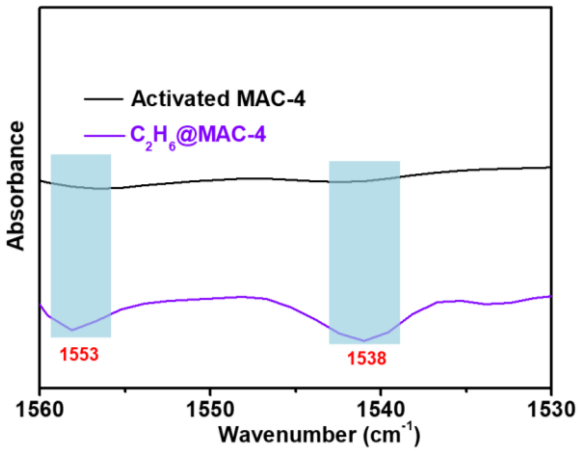


**Figure S48.** Comparison of IR spectra at 1560-1530 $cm^{-1}$ of activated and $C_2H_6$-loaded MAC-4.

## References

[1] Y. Ling, F. Yang, M. Deng, Z. Chen, X. Liu, L. Weng, Y. Zhou, *Dalton Trans*. **2012**, *41*, 4007-4011.

[2] *R. Krishna*, *RSC Adv.* **2017**, *7*, 35724-35737.

[3] R. Krishna, *ACS Omega* **2020**, 5, 16987−17004.

[4] R. Krishna, *Microporous Mesoporous Mater.* **2014**, *185*, 30-50.

[5] R. Krishna, *RSC Adv.* **2015**, *5*, 52269-52295.

[6] R. Krishna. *Sep. Purif. Technol.* **2018**, *194*, 281-300.

[7] R. Krishna. *Precision Chemistry* **2023**, *1*, 83-93.

## Author contributions

**Gang-Ding Wang:** Synthesis, characterization, adsorption experiments, writing - original draft. **Yong-Zhi Li:** Breakthrough experiments, writing - review & editing. **Rajamani Krishna:** Breakthrough simulation**,** $Q_{st}$ calculation. **Wen-Yan Zhang:** Formal analysis. **Lei Hou:** Formal analysis, writing - review & editing, supervision, methodology, funding acquisition. **Yao-Yu Wang:** Resources. **Zhonghua Zhu:** Formal analysis.